(Preprint) AAS 25-886

SUMMARIZING RELATIVE MOTION NEAR PERIODIC ORBITS WITH MOTION PRIMITIVES

Maxwell Joyner* **and Natasha Bosanac** †

This paper focuses on using motion primitives to summarize relative motion in the neighborhood of a target vehicle that is located along a periodic orbit in the Earth-Moon circular restricted three-body problem. These relative trajectories are generated near states along various libration points and Moon-centered orbits. Then, each trajectory is transformed into a suitable reference frame and discretized. The sampled states are used to form finite-dimensional feature vectors that are clustered to generate groups of geometrically similar relative trajectories. A motion primitive is extracted from each cluster to explore fundamental types of relative motion in cislunar space.

INTRODUCTION

Orbital rendezvous operations in cislunar space are becoming an increasingly common element of space operations. NASA's Artemis missions currently plan for docking and crew transfer between the Orion spacecraft and the Human Landing System in an Earth-Moon L_2 halo orbit.[1] The Lunar Gateway station is expected to eventually function as a rendezvous hub occupying a similar orbit. Although orbital rendezvous has become nearly routine in low-Earth orbit (LEO), the more complex dynamics in cislunar space limit the applicability of heritage approaches to describing, analyzing, and designing motions for a chaser vehicle relative to a target vehicle.

Relative motion is studied via the trajectory of a chaser spacecraft measured relative to the state of a target spacecraft. The well-known Clohessy-Wiltshire equations for studying relative motion cannot be accurately applied to a multi-body system.[2] Alternatively, the nonlinear dynamics of a multi-body gravitational system may be linearized about the target, as performed by Luquette and Sanner.[3] However, Franzini and Innocenti demonstrated that they are sensitive to perturbations and the accuracy of linear approximations decreases rapidly with increasing state deviations from the target.[4] Accordingly, Franzini and Innocenti formulated equations of relative motion in the Earth-Moon circular restricted three-body problem (CR3BP) using the well-known local vertical, local horizontal (LVLH) frame relative to the Moon.[5] Based on the use of the LVLH frame in studying relative motion in LEO, the origin is located at the target and the axes are calculated using the position vector and orbital angular momentum of the target relative to a central body.[6] However, in the CR3BP, periodic orbits can revolve around equilibrium points or multiple reference points, limiting the applicability of these axes. Motion relative to a target along a periodic orbit in the CR3BP has also been studied using the structure of its local neighborhood. For example, Hsiao

*Graduate Researcher, Colorado Center for Astrodynamics Research, Smead Department of Aerospace Engineering Sciences, University of Colorado Boulder, Boulder, CO, 80303.

†Associate Professor, Colorado Center for Astrodynamics Research, Smead Department of Aerospace Engineering Sciences, University of Colorado Boulder, Boulder, CO 80303.

and Scheeres used information about the eigenspace of a periodic orbit to introduce linear orbital elements.[7] Elliott and Bosanac built upon this foundation to define local toroidal coordinates that use approximations of the invariant tori of a target periodic orbit to form a geometric description of relative motion.[8] However, when trajectories are generated in models of higher-fidelity, with continuous thrust, around complex and non-periodic trajectories, and/or over time-spans that violate the assumptions of linearization, more generalizable procedures for studying and describing a diverse array of relative motions can be valuable.

A variety of technical disciplines have addressed similar challenges in summarizing motions in complex dynamical environments. In robotics, motion primitives have been defined as the building blocks of motion.[9] A library of these motion primitives, extracted from observations or simulated data, can supply a digestible summary of the solution space. Sequences of these motion primitives have also supported rapid design or the prediction of paths for robotics, humans, or animals.[10]

In astrodynamics, motion primitives have recently been used to design complex spacecraft trajectories within multi-body gravitational systems and explore the associated tradespace. For this application, Smith and Bosanac introduced a motion primitive as a single trajectory that summarizes a set of neighboring trajectories in the phase space with a similar geometry.[11] A proof of concept was presented for periodic orbits and arcs along hyperbolic invariant manifolds of periodic orbits in the Earth-Moon CR3BP.[12] Specifically, clustering was used to group arcs from each type of fundamental solution by their geometry. Then, a single representative member of each group supplies a motion primitive. More recently, Gillespie, Miceli, and Bosanac built upon this foundation to 1) calculate groups of geometrically similar periodic orbits as continuous segments of a family with the same number of maxima in the curvature, and 2) present an updated clustering approach that generates more accurate groupings of arcs along natural or thrust-enabled trajectories that approach or depart a periodic orbit.[13] Smith and Bosanac also demonstrated the construction of a motion primitive graph that can be searched to generate primitive sequences.[12] These sequences are then refined to produce initial guesses that are corrected to continuous trajectories.[12] Recently, Miceli and Bosanac have improved upon this motion primitive approach to trajectory design by defining an updated graph structure, k-best paths search algorithm, and refinement process to generate a geometrically diverse array of transfers within a multi-body system.[14] These works have demonstrated that a library of motion primitives is capable of summarizing a segment of the solution space in the CR3BP and support rapid and efficient trajectory design space exploration in a complex gravitational environment. This paper leverages this prior work as a foundation, but builds upon it through an application to relative motion between two spacecraft.

This paper focuses on generating relative motion primitives for spacecraft operating near periodic orbits in the Earth-Moon CR3BP. These motion primitives capture fundamental modes in the relative motion problem which can, eventually, support rapid rendezvous trajectory design. First, trajectories are generated and described for a spacecraft that operates near a target vehicle located along several example periodic orbits in the CR3BP. Multiple approaches to sampling spacecraft paths are evaluated to identify a new finite-dimensional description of continuous relative trajectories that sufficiently captures their geometries. Then, a two-step clustering process is applied to automatically extract groups of arcs with a similar geometry. A single representative trajectory is then extracted from each group to form the relative motion primitive. After generating a library of relative motion primitives that summarize the solution space, the fundamental types of relative motion near the selected periodic orbits are examined.

BACKGROUND

Circular Restricted Three-Body Problem

The Circular Restricted Three-Body Problem (CR3BP) is used to approximate motion of each spacecraft in cislunar space. The Earth (P_1) and Moon (P_2) are modeled with the same gravitational field as point masses, following circular orbits about their barycenter.[15] The masses of spacecraft in this system are assumed to be negligible compared to the constant masses of primaries P_1 and P_2.

States and parameters are typically nondimensionalized in the CR3BP using characteristic length, mass, and time quantities. The characteristic length is set to the average separation between the Earth and the Moon, equivalent to $l^* = 384,000\ km$. The total mass of the Earth and Moon is set as the characteristic mass, $m^* \approx 6.046804 \times 10^{24}\ kg$. Finally, the characteristic time is set to $t^* \approx 3.751903 \times 10^5\ s$ to produce a mean motion of the primaries equal to unity.

Trajectories in the CR3BP are analyzed in a rotating frame. The origin is placed at the barycenter of P_1 and P_2. The axes are defined with $\hat{x}$ directed along the line from P_1 to P_2, $\hat{z}$ aligned with the orbital angular momentum vector, and $\hat{y}$ completing the right-handed, orthogonal triad.[15]

The nondimensional equations of motion for the CR3BP are formulated in the rotating $P_1 - P_2$ frame. A state vector is defined for a spacecraft as $\bar{x} = [x, y, z, \dot{x}, \dot{y}, \dot{z}]^T$. Equations of motion[15] are then succinctly written as

$$\ddot{x} = 2\dot{y} + \frac{\partial U^*}{\partial x}, \quad \ddot{y} = -2\dot{x} + \frac{\partial U^*}{\partial y}, \quad \ddot{z} = \frac{\partial U^*}{\partial z} \tag{1}$$

using the pseudopotential function U^*, equal to

$$U^* = \frac{1}{2}\left(x^2 + y^2\right) + \frac{1-\mu}{r_1} + \frac{\mu}{r_2} \tag{2}$$

where $r_1 = \sqrt{(x+\mu)^2 + y^2 + z^2}$ and $r_2 = \sqrt{(x-1+\mu)^2 + y^2 + z^2}$ are the distances of the spacecraft from the primaries P_1 and P_2 whereas the mass ratio μ represents the mass of the smaller primary over the total mass of both bodies. For the Earth-Moon system, $\mu \approx 0.012151$. Although no analytical solution to the CR3BP exists, an integral of motion C_J equals

$$C_J = 2U^* - \dot{x} - \dot{y} - \dot{z} \tag{3}$$

This energy-like constant C_J is labeled the Jacobi constant.

A variety of fundamental solutions exist in the autonomous CR3BP.[15] Five equilibrium solutions, L_1-L_5 known as libration points or Lagrange points exist in the CR3BP as stationary solutions in the rotating frame. Trajectories that repeat their motion over a constant time period in the rotating frame are defined as periodic orbits. These periodic orbits exist in continuous families within various regions of the system. Finally, hyperbolic invariant manifolds associated with libration points or periodic/quasi-periodic orbits capture trajectories that asymptotically depart (unstable manifold) or approach (stable manifold) these solutions.

Relative Motion in the Circular Restricted Three-Body Problem

Relative motion in the CR3BP is described using the standard definitions of target and chaser spacecraft.[2] A passive target spacecraft (denoted by the subscript t) travels along its orbit while the

active chaser spacecraft (denoted by the subscript c) approaches or departs its vicinity. The relative state vector, and its time derivatives, of the chaser spacecraft is expressed with respect to the target vehicle as

$$\bar{r}_c = \bar{R}_c - \bar{R}_t \ , \ \bar{v}_c = \bar{V}_c - \bar{V}_t \ , \ \bar{a}_c = \bar{A}_c - \bar{A}_t \tag{4}$$

A 12-dimensional vector composed of the absolute state of the target spacecraft along with the relative state of the chaser spacecraft with respect to the target is defined as

$$\bar{x}_{full} = [X_t, Y_t, Z_t, \dot{X}_t, \dot{Y}_t, \dot{Z}_t, x_c, y_c, z_c, \dot{x}_c, \dot{y}_c, \dot{z}_c] \tag{5}$$

The relative equations of motion for the chaser are thenwritten as[15]

$$\ddot{x}_c = \left(2\dot{Y}_c + \frac{\partial U_c^*}{\partial X_c}\right) - \left(2\dot{Y}_t + \frac{\partial U_t^*}{\partial X_t}\right) \tag{6}$$

$$\ddot{y}_c = \left(-2\dot{X}_c + \frac{\partial U_c^*}{\partial Y_c}\right) - \left(-2\dot{X}_t + \frac{\partial U_t^*}{\partial Y_t}\right) \tag{7}$$

$$\ddot{z}_c = \frac{\partial U_c^*}{\partial Z_c} - \frac{\partial U_t^*}{\partial Z_t} \tag{8}$$

where U_t^* and U_c^* are equal to the pseudopotential function evaluated using the absolute state vectors of the target and chaser spacecraft, respectively.

Curvature

Nonlinear trajectories are analyzed and described using concepts from differential geometry. These techniques are defined using the instantaneous position, velocity, and acceleration vectors of a curve, $\bar{r}(t) = [x(t), y(t), z(t)]^T$, $\bar{v}(t) = [\dot{x}(t), \dot{y}(t), \dot{z}(t)]^T$, and $\bar{a}(t) = [\ddot{x}(t), \ddot{y}(t), \ddot{z}(t)]^T$, respectively. Beginning from an initial state, a trajectory generated over the time interval $t \in [t_0, t_f]$ traversed a distance s equal to the arclength[16]

$$s = \int_{t_0}^{t_f} ds = \int_{t_0}^{t_f} \sqrt{\dot{x}^2 + \dot{y}^2 + \dot{z}^2} dt \tag{9}$$

The instantaneous curvature $\kappa(t)$ quantifies the deviation of a path from a straight line in the osculating plane, defined as the plane formed by three points along the curve as the limit of the arclength between them approaches zero.[17] For a given point along a trajectory, the corresponding state vectors can be used to express the curvature mathematically as

$$\kappa(t) = \frac{\|\bar{v}(t) \times \bar{a}(t)\|}{\|\bar{v}(t)\|^3} = \frac{\sqrt{(\ddot{z}\dot{y} - \ddot{y}\dot{z})^2 + (\ddot{x}\dot{z} - \ddot{z}\dot{x})^2 + (\ddot{y}\dot{x} - \ddot{x}\dot{y})^2}}{(\dot{x}^2 + \dot{y}^2 + \dot{z}^2)^{3/2}} \tag{10}$$

with a singularity when the speed equals zero.

Geometrically significant locations along a trajectory can be located through tracking where maxima in this curvature value occur.[17] Curvature maxima occur when $\dot{\kappa} = 0$ and $\ddot{\kappa} < 0$. For multi-body systems, these curvature maxima can be located near apses defined with respect to points of interest in the CR3BP such as primary bodies or libration points.[18] Curvature maxima can also be located along curves in the relative CR3BP, where they can exist near points of local minima or maxima in the relative distance of the chaser spacecraft with respect to the target.

Curve-Based Reference Frames

Reference frames based on the shape of spatial curves are often employed in differential geometry and computer graphics. These curve-based frames consist of axes constructed using the local geometry of a curve as opposed to the location of the trajectory in configuration space used in reference frames like the Velocity-Normal-Conormal (VNC) axes.[19] Curve-based reference frames can be useful for trajectories in the CR3BP that traverse multiple regions of the system. The Frenet frame is an example that is defined based on the curvature. The axes are defined using the tangent vector $\hat{T}$ parallel to the velocity unit vector, the normal vector $\hat{N}$ directed towards the center of curvature in the osculating plane, and the binormal vector $\hat{B}$ normal to the osculating frame to complete the right-handed coordinate frame.[16] When the curvature is non-zero ($\kappa \neq 0$), the Frenet unit axes are calculated from the position vector and its time derivatives as

$$\hat{T} = \frac{\bar{v}}{|\bar{v}|} = \frac{\dot{\bar{r}}}{|\dot{\bar{r}}|}, \quad \hat{N} = \hat{B} \times \hat{T}, \quad \hat{B} = \frac{\bar{v} \times \bar{a}}{|\bar{v} \times \bar{a}|} = \frac{\dot{\bar{r}} \times \ddot{\bar{r}}}{|\dot{\bar{r}} \times \ddot{\bar{r}}|}$$

Density-Based Clustering

Clustering algorithms are used to discover groupings within a dataset.[20] Individual members of the dataset are first summarized using finite-dimensional feature vectors representing relevant attributes related to the desired sorting criteria. The clustering algorithm then groups or separates these feature vectors based on the distance between them calculated using a specified distance metric, with similar members grouped closer together and dissimilar members lying further apart. Although a variety of approaches to clustering exist, this paper uses two density-based clustering algorithms for their suitability in identifying irregularly shaped clusters: 1) Density-Based Spatial Clustering of Applications with Noise (DBSCAN)[21] and 2) Hierarchical Density-Based Spatial Clustering of Applications with Noise (HDBSCAN).[22]

DBSCAN was developed by Ester, Kriegel, Sander, and Xu to group dense regions of data with overlapping neighborhoods of a user-specified radius.[21] The m_{pts}-neighborhood of a member of the dataset is defined as a hypersphere that encompasses its m_{pts}-th nearest neighbors. This member is classified as a core point if these neighbors lie within a specified radius ϵ. If fewer than m_{pts} members lie within a distance of ϵ but they include another core point, the member is defined as a border point. However, if neither of these criteria are satisfied, the member is labeled as a noise point. Core points and their associated border points are then grouped together as clusters if their neighborhoods overlap. DBSCAN is useful when suitable values for m_{pts} and ϵ can be selected. For this paper, DBSCAN is accessed through the MATLAB library.

HDBSCAN was developed by Campello, Moulavi, and Sander to extend the density-based approach of DBSCAN.[22] Similar data points are first identified in dense local neighborhoods, then groupings of clusters are formed through hierarchical association with each other. This approach is useful when the neighborhood size or local density of a data set are not known a priori. HDBSCAN formulates the similarity or dissimilarity between two data points through a mapping into the mutual reachability distance. The core distance for each member of a data set is defined as the distance to its m_{pts}-nearest neighbor using a specified distance metric. For any two points, the mutual reachability distance is then defined as the maximum value of the distance between them and either of their respective core distances.

A weighted graph is constructed from the data points with each edge weight representing the mutual reachability distance between all pairwise combinations of data points.[22] The connections in

this graph are then summarized using a minimum spanning tree. This tree is further condensed into a hierarchical tree ranked by mutual reachability distance, where each node represents a potential cluster. Stable clusters with at least $m_{clust,min}$ members are then extracted from this condensed tree based on the criteria of maximizing the excess of mass.[22] HDBSCAN assigns all data points in dense neighborhoods as cluster members or labels them as noise if they lie within insufficiently dense regions of the mutual reachability distance space. An additional modification to the HDBSCAN introduces a distance threshold ϵ_{merge} to join two data points below this value together in the same cluster to prevent excessive subdivision beyond a desired resolution.[23] For this paper, HDBSCAN is accessed through the $hdbscan$ Python library.[24]

TECHNICAL APPROACH

Relative Motion Primitives

Spacecraft rendezvous in cislunar space is dependent on the complex dynamics governing their motion in this gravitational environment. Periodic orbits in the CR3BP also exhibit a much wider diversity of geometry compared to the near-circular orbits for target spacecraft typical of rendezvous in LEO. Both of these factors require the development of new strategies to characterize the design space for relative motion. This paper builds upon prior work by Smith and Bosanac[12] as well as Miceli and Bosanac[14] in applying the motion primitive concept to relative trajectory design in multi-body systems. However, relative motion near periodic orbits in the CR3BP possess their own distinct geometric characteristics on time and distance scales that differ from those used for absolute motion. Thus, these characteristics require the development of a modified technical approach for seeding initial conditions, propagating and sampling the associated trajectories, and clustering the resulting feature vectors for identifying relative motion primitives.

Step 1: Generating initial target spacecraft states

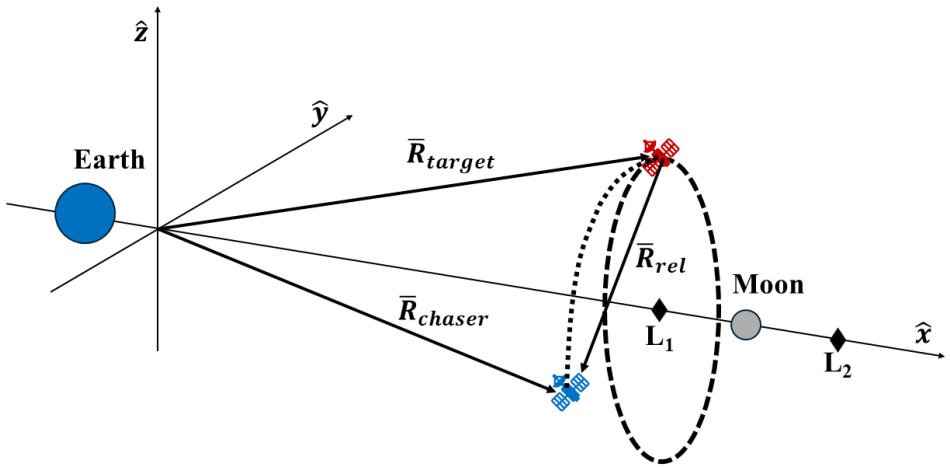

Figure 1. Target spacecraft occupying a periodic orbit about L_1 and nearby chaser spacecraft with a relative state $\bar{X}_{rel}$ in the Earth-Moon CR3BP.

In this paper, the positions of target spacecraft are constrained to natural motion along periodic orbits in the Earth-Moon CR3BP. These target states are used to define the relative state of a chaser spacecraft as depicted in Figure 1. In the context of future exploration efforts, orbits in the vicinity

of the Moon are of particular interest for placing rendezvous targets such as orbital platforms or refueling stations.[1] Families of planar and spatial periodic orbits near the libration points L_1 and L_2 (Lyapunov, halo, vertical and axial) as well as those centered around the Moon (distant prograde orbits, low prograde orbits, and distant retrograde orbits) are explored to provide a diversity of geometric and stability characteristics. For this proof of concept, a single member is selected as an example from each periodic orbit family. The attributes of these example periodic orbits are summarized in Table 1. The speed and distance from the secondary body may vary substantially along many periodic orbits in the CR3BP. These factors significantly impact the relative motion behavior of a chaser spacecraft. To sufficiently capture the design space of the resulting chaser trajectories, a set of initial target states is sampled from the orbits selected for this analysis. This approach distributes nodes equally spaced in arclength along the periodic orbit. These nodes represent initial or final states for a target spacecraft.

Table 1. Orbital period, Jacobi constant, and stability indices for example periodic orbits.

Orbit	Period (n.d.)	Period (days)	Jacobi Constant	s_1	s_2
L_2 Lyapunov Orbit	3.6485	15.84	3.0864	1156.84	2.17
L_1 Halo Orbit	2.6194	11.37	3.0143	-1.933	34.69
L_1 Vertical Orbit	3.8240	16.61	3.0153	1.80	627.16
L_2 Axial Orbit	4.3954	19.09	2.9771	319.14	2.26
L_2 Southern NRHO	1.5151	6.58	3.0462	1.02	-0.18
Distant Prograde Orbit	2.1743	9.44	3.1713	-1.96	-0.53
Low Prograde Orbit	0.6188	2.69	3.2648	1.58	1.7344
Distant Retrograde Orbit	1.3541	5.88	3.0178	0.47	0.94

Step 2: Generating initial chaser spacecraft relative states

Initial chaser positions are then defined relative to the target for each of the target states generated in the previous step. Previous investigations have revealed a strong dependence on the orientation of the chaser displacement with respect to the target's unit velocity vector in the rotating frame on the resulting relative motion behavior.[25,26] Position displacements are therefore consistently defined around the target's direction of motion for any point along each periodic orbit. The Frenet frame axes are first calculated for a given target state. The basis vectors $\hat{X}\hat{Y}\hat{Z}$ are defined using the target's Frenet axes such that the $\hat{Z}$ axis is parallel to $\hat{T}$, $\hat{X}$ is aligned with $\hat{N}$, and $\hat{Y}$ is aligned with $\hat{B}$. Points along the surface of a unit sphere are then spaced at equal angular intervals with increments of $\theta_{IP,r} = 30^\circ$ about the $\hat{T}$ axis in the $\hat{N} - \hat{B}$ plane and increments of $\theta_{OOP,r} = 30^\circ$ offset from the $\hat{N} - \hat{B}$ plane. Each position defined along this unit sphere is then multiplied by a desired range value $\|d\bar{r}\|$ to produce a set of chaser position vectors with equivalent distances from the target spacecraft. This work uses a value of $\|d\bar{r}\| = 10\ km$, consistent with the boundary of the

rendezvous sphere concept employed in collision avoidance analysis for the Lunar Gateway.[27]

A set of initial chaser relative velocities for each relative position is defined using a similar unit sphere approach. The $\hat{Z}$ axis is rotated to align with the relative position vector $\hat{r}_c$ and the $\hat{X}$ and $\hat{Y}$ axes lie within a plane tangent to the surface of the sphere. Equal angular intervals with increments of $\theta_{IP,v} = 15^\circ$ about the $\hat{r}_c$ axis and increments of $\theta_{OOP,v} = 15^\circ$ offset out of the plane are used to define unit velocity vectors. These vectors are then multiplied by a speed $d\bar{v}_c$ to obtain an initial relative velocity with respect to the target. In this paper, the magnitudes used are selected from the set $\|d\bar{v}_c\| = [0.5,\ 1,\ 2,\ 5]\ m/s$ based on typical values for periodic orbit rendezvous.[25] The results are analyzed individually for each relative speed due to the large dependence of the initial velocity on the resulting relative trajectory geometry. Finally, initial conditions generated for the target and

Table 2. Summary of values used to generate initial values for relative chaser position and velocity.

	θ_{IP}	θ_{OOP}	Total Samples	Magnitude
Relative Position $d\bar{r}$	30°	30°	62	$10\ km$
Relative Velocity $d\bar{v}$	15°	15°	266	$0.5, 1, 2, 5\ m/s$

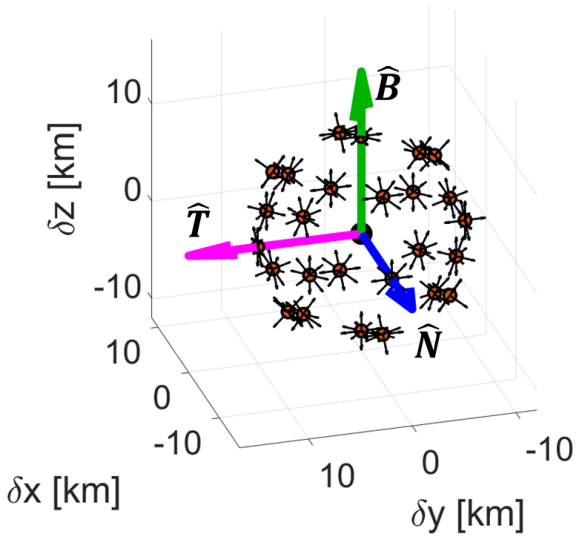

Figure 2. Example chaser relative positions (orange) and their associated relative velocities (black arrows) generated with respect to the target and local Frenet axes

chaser spacecraft are combined into complete state vectors. The chaser displacement magnitudes for $\|d\bar{r}\|$ and $\|d\bar{v}\|$ are conveniently defined in km and m/s for clarity, but are nondimensionalized using the characteristic length and time values for the Earth-Moon system. Each target state is associated with a set of chaser positions and their corresponding set of chaser velocities, producing $16,492$ chaser relative states for each target. An illustration of this concept with larger angular intervals for clarity is shown in Figure 2, while the actual values used are summarized in Table 2.

Step 3: Propagate initial conditions and collect samples for feature vectors

Full state vectors containing the absolute target state and relative chaser state are integrated using their respective equations of motion to generate sets of relative motion trajectories. Each set of initial conditions is propagated twice: 1) forward in time to represent a chaser spacecraft departing from an initial state and 2) backward in time for an approaching chaser spacecraft reaching the condition as a final state. Two termination conditions are enforced when critical ranges from the target spacecraft are reached: 1) $\|\bar{r}_{c,out}\| = 2000\ km$ for the chaser spacecraft departing or approaching the relative motion regime surrounding the target spacecraft, and 2) $\|\bar{r}_{c,in}\| = 0.2\ km$ when the chaser crosses into a keep-out sphere surrounding the target.[28] The larger boundary value is chosen to constrain a region where relative motion is applicable while still allowing for an overlap with far-range motion for connection in future work. An additional constraint when 10 time units have elapsed is also necessary for stable orbits to prevent excessive computational time.

To discretely summarize the relative motion trajectories and capture their geometric characteristics, a variety of approaches for sampling states are evaluated, as illustrated in Figure 3. A range-based method collects samples when the chaser spacecraft reaches critical user-defined distance values while approaching or departing from the target. Similarly, an approach using critical user-defined values of arclength as the chaser travels along a path is implemented. Curvature maxima events where the derivative $\frac{\partial \kappa}{\partial t} = 0$ are also explored as sampling criteria. Two approaches using 1) curvature maxima alone 2) both curvature maxima and minima to identify sample locations are tested. Finally, a hybrid approach incorporates samples from both maximum curvature events and even intervals of arclength between them. This procedure is based on work by Gillespie, Miceli, and Bosanac,[13] but multiple values of intervals are evaluated and both the initial and final state are treated as curvature events if none exist for arclength intervals to ensure that every trajectory is sampled at least once.

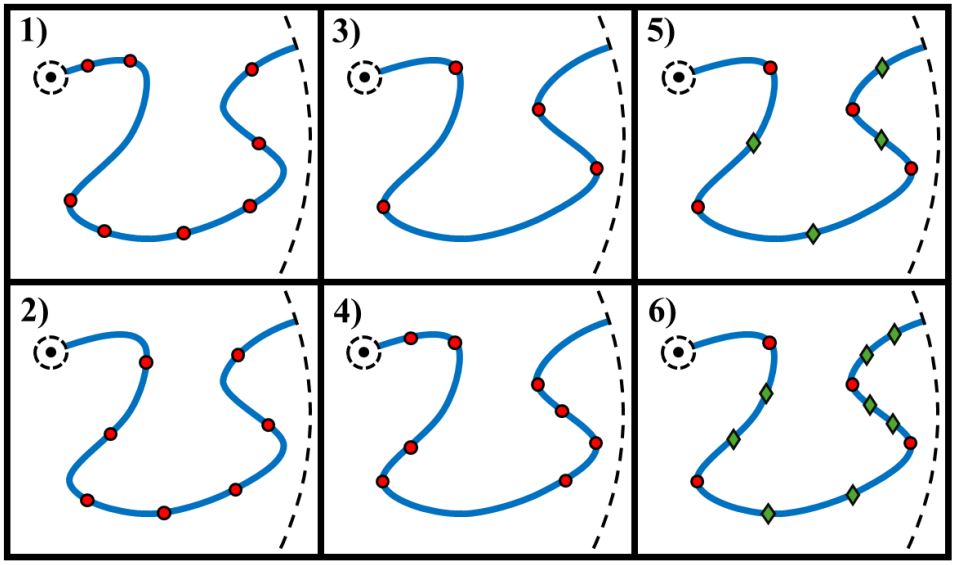

Figure 3. Various approaches to sampling chaser spacecraft states in relative motion trajectories, including 1) range-based, 2) arclength-based, 3) maximimum curvature, 4) maximum and minimum curvature, 5) maximum curvature with one arclength sample, and 5) maximum curvature with two arclength samples

For each approach, the resulting samples are assembled into finite-dimensional feature vectors to summarize each relative motion trajectory for the clustering process. State information at each sampled state is used to construct two feature vectors: the position-based vector is defined as

$$\bar{f}_p = [x_1, y_1, z_1, \ldots, x_{N_s}, y_{N_s}, z_{N_s}]$$

whereas the velocity-based vector is defined as

$$\bar{f}_v = \left[\tilde{\dot{x}}_1, \tilde{\dot{y}}_1, \tilde{\dot{z}}_1, \ldots, \tilde{\dot{x}}_{N_s}, \tilde{\dot{y}}_{N_s}, \tilde{\dot{z}}_{N_s}\right]$$

where $\tilde{\dot{x}}$ denotes the normalized unit velocity components used to capture the shape of each trajectory. Normalization promotes feature vectors that represent path geometry regardless of speed.

Step 4: Cluster and select primitives

Relative motion trajectories generated for a chaser spacecraft are clustered to identify groups with similar geometry for selecting motion primitives. The two sets of departing and approaching paths are each processed separately. Trajectories are also sorted into partitions with equal numbers of samples prior to clustering, since the algorithms require feature vectors with an equivalent number of dimensions. To ensure high-quality clustering results for a variety of geometries, a two-step clustering approach originally developed by Bosanac[29] and then used by Gillespie, Miceli, and Bosanac[13] is adapted for relative motion trajectories.

Departing and approaching paths are first coarsely clustered by processing each set of shape-based feature vectors $\bar{f}_v$ with the HDBSCAN algorithm. This step supports grouping trajectories with a diverse array of densities and configurations to be identified without a priori knowledge of their distribution or membership sizes.[22] Feature vectors are clustered using a Euclidean distance metric, with HDBSCAN parameters set to $m_{min,clust} = 5$ and $m_{pts} = 4$[29] to emphasize the selection of smaller localized clusters. The epsilon threshold ϵ used to constrain the neighborhood size used to distinguish between individual clusters is heuristically defined as $\epsilon = 2\sqrt{N_s}sin(\Delta\theta/2)$,[29] where $\Delta\theta = 10^\circ$ is a limit on the average angle between velocity unit vectors and is scaled by the N_s number of samples for the given set of relative motion trajectories. This initial course clustering step produces groupings with roughly similar shapes; any unlabeled points are discarded as noise.

An additional cluster refinement step is applied to further ensure high-quality groupings of relative motion trajectories by removing outliers. This process is based on a convoy detection approach in the trajectory clustering literature.[30] Convoy detection works by analyzing each set of sample points along a trajectory sequentially to identify groupings that remain density-connected for their entire duration. First applied to trajectories in the CR3BP by Bosanac,[29] this approach is adapted for relative motion trajectories.

Each cluster of relative motion trajectories identified in the previous step is individually refined through a convoy detection process.[29] For the i-th sample along each set of paths, two three-dimensional feature vectors $\bar{f}_{v,i}$ and $\bar{f}_{p,i}$ are formed to represent the associated state. These two feature vectors are then independently clustered with DBSCAN and a Euclidean distance measure for $m_{pts} = 4$ and $\epsilon = m_{pts}max(e, \epsilon_{threshold})$.[29] Here, e is the median distance of each subset of feature vectors from their nearest neighbors and $\epsilon_{threshold}$ is a minimum threshold value. This local neighborhood size is selected to be large enough to allow the DBSCAN algorithm to locate a sufficient number of core points without excessive bias from outliers. This process is repeated for all subsequent N_s samples using both shape-based $\bar{f}_{v,i}$ and position-based $\bar{f}_{p,i}$ for a total of

$2N_s$ convoy detection steps. If a set of relative motion trajectories is grouped together for all $2N_s$ clustering results, they form a refined cluster. The previous coarse clusters may be subdivided into multiple refined clusters, but if a feature vector associated with any sample is labeled as noise, then the entire trajectory is discarded. Performing this clustering step independently for each sample ensures that the sets of refined clusters are composed of relative motion trajectories that possess similar geometry for their entire duration.

Relative motion primitives are extracted by selecting a representative from each refined cluster. Each representative trajectory is selected as the medoid of its cluster,[12] which is expressed mathematically as

$$\bar{f}_{medoid} = \min_{\bar{f}_i \in \mathcal{F}} \left(\sum_{j=1}^{\mathcal{F}} \|\bar{f}_i - \bar{f}_j\| \right)$$

This medoid is calculated in the position-based feature vector space.

The resulting clusters of relative motion trajectories are visualized by displaying their constituent members along with the representative motion primitive. Each primitive is plotted using a thicker and darker line to distinguish them, with a gray line depicting a two-dimensional projection at the bottom of the plot. Trajectories departing from the vicinity of the target spacecraft are red, while those approaching the target are blue. The shade of these colors is used to indicate the speed at the critical range $\|\bar{r}_{c,out}\|$ from the target, with slower trajectories plotted in lighter shades and faster trajectories as darker shades. The positions at critical range $\|\bar{r}_{c,out}\|$ for departing and approaching trajectories are displayed as points of their respective color. Relative motion trajectories are plotted using the same axes in the rotating frame defined for the CR3BP but shifted so that the target lies at the origin. The target's direction of motion at the time of initial departure or final approach is represented by a black arrow.

RESULTS

The outlined technical approach is applied to a variety of representative periodic orbits in cislunar space. Several sampling approaches are tested with the clustering process to determine an appropriate methodology for capturing the geometry of trajectories in relative motion. The resulting samples and clusters are compared for the same test case and the most suitable sampling approach is identified. Next, this approach is used to generate motion primitives for relative motion trajectories near several periodic orbits in the Earth-Moon CR3BP. Selected clusters of departing and approaching trajectories for each orbit are presented and discussed.

Evaluating Sampling Approaches

Multiple strategies for selecting appropriate sample locations are implemented for chaser spacecraft trajectories near a target in an L_1 halo orbit at apolune with $\|d\bar{v}_c\| = 1\ m/s$. Each set of samples is then assembled into feature vectors and clustered using the same process. Statistics for samples, clusters, and computational data for sampling approaches using set range and arclength intervals as well as curvature extrema are summarized in Table 3. A Windows machine with 16GB RAM and an AMD Ryzen 5 5600G processor is used for computation, and storage size includes all sample states along with trajectory summaries. Range samples are taken when values of $100 : 100 : 1000\ km$ are reached from the target spacecraft, while arclength samples are collected at values $100 : 200 : 1000\ km$ and $3000 : 1000 : 20000\ km$ along the chaser trajectory. Two sets of samples are taken when $\frac{\partial \kappa}{\partial t} = 0$ at maximum and both minimum and maximum curvature events.

Table 3. Sample and clustering statistics for chaser spacecraft trajectories near a target in an L_1 halo orbit at apolune using range-based, arclength-based, and curvature-based sampling approaches

Sampling Approach	Range	Arclength	Max. Curvature	Max. + Min. Curv.
Min. # of Samples	10	5	0	1
Max. # of Samples	24	21	9	18
Median # of Samples	10	7	2	4
Noise (%)	45.1	25.5	17.1	22.8
# of Clusters	329	286	238	351
Max. Cluster Size	1418	1041	1219	1110
Median Cluster Size	8	10	9	8
Computational Time (s)	139.1	71.0	37.0	54.0
Storage Size (MB)	16.5	11.0	4.9	8.3

Each of these sampling approaches has strengths and drawbacks when implemented individually. Range-based sampling aligns with how actual chaser vehicles, such as Orion, switch between operational procedures based on distance from a target.[28] However, behavior where a trajectory remains at the same approximate range while traveling about the target results in an undersampling of these regions. This is consistent with the high percentage of discarded trajectories. Arclength-based sampling produces higher-quality clusters, but defining specific sample values for a wide range of different geometries is challenging. Regions of maximum curvature often correspond to locations where the chaser spacecraft reaches a local minimum or maximum distance from the target spacecraft. These are geometrically significant locations that are also of interest for rendezvous and proximity operations. However, this criterion produces a lower number of samples and, for some trajectories, no samples at all. Augmenting this approach by adding minimum curvature events results in a higher number of samples, but these regions are often less significant for describing the geometry of the trajectory.

A hybrid sampling methodology incorporates both maximum curvature events and samples at intervals of equal arclength between them to leverage the advantages of both approaches; this approach was previously developed by Gillespie, Miceli, and Bosanac.[13] This approach simplifies the task of defining specific arclength values into a single variable that specifies the number of equal interval samples, N_{AL}. Several values of N_{AL} are evaluated using the same conditions from the previous example for comparison, summarized in Table 4. Although the number of samples, computational time, and storage size predictably increase with larger values of N_L, the total number of clusters as well as the maximum and median cluster size remain consistent. The percentage of trajectories discarded as noise increases slightly with additional arclength samples. From these results, increasing the value of N_{AL} does not fundamentally alter cluster assignments but does provide the clustering process additional data to remove outliers.

Table 4. Sample and clustering statistics for chaser spacecraft trajectories near a target in an L_1 halo orbit at apolune using a hybrid maximum curvature/arclength interval approach for several N_{AL}.

Max. Curv. + N_{AL} Arc Length Sample	1	2	3	4
Min. # of Samples	1	2	3	4
Max. # of Samples	18	27	36	45
Median # of Samples	4	6	8	10
Noise %	22.8	27.9	29.5	30.5
# of Clusters	247	248	247	252
Max. Cluster Size	1177	1178	1145	1138
Median Cluster Size	9	8	8	8
Computational Time	89.1	109.4	129.7	156.9
Storage Size	7.9	11.7	15.6	19.3

Table 5. Sample and clustering statistics for chaser spacecraft trajectories near a target in an L_1 halo orbit at apolune for several values of $\|d\bar{v}_c\|$.

Initial Relative Speed $\|d\bar{v}_c\|$ (m/s)	0.5	1	2	5
Min. # of Samples	3	2	2	2
Max. # of Samples	39	27	36	21
Median # of Samples	9	6	6	3
Noise %	23.5	27.9	27.0	30.6
# of Clusters	195	248	391	628
Max. Cluster Size	1452	1178	925	1172
Median Cluster Size	8	8	10	8

Finally, the hybrid sampling approach employing both maximum curvature events and $N_{AL} = 2$ samples of equal arc length between them is tested using the same scenario with multiple initial chaser speeds $\|d\bar{v}_c\|$ to evaluate the performance for a more diverse set of geometries. Larger initial values of $\|d\bar{v}_c\|$ are correlated with a lower number of samples as the chaser spacecraft tends to exit the region surrounding the target the target more rapidly. These trajectories are also observed to traverse paths with less curvature, resulting in fewer maximum curvature events. However, the number of clusters identified increases significantly for larger values of $\|d\bar{v}_c\|$. While chaser trajectories travel along straighter paths away from the target and visually resemble one another, additional re-

gions in the design space become reachable by the chaser to create a larger range of spatial diversity.

The percentage of relative motion trajectories discarded as noise is considerably high for this approach. One potential explanation may be the choice of initial conditions used to generate relative motion trajectories. Many maximum curvature events are observed near the target, which may present challenges for the clustering algorithm to group trajectories based on samples. Additionally, the increased degree of geometric diversity observed near apolune is a potential factor complicating the process of grouping trajectories.

Summarizing Relative Motion to/from Various Orbits

The selected sampling approach is used to generate motion primitives that summarize relative motion trajectories near several periodic orbits. The initial relative speed of the chaser spacecraft is set as $\|d\bar{v}_c\| = 1\ m/s$ for all cases in this section. Clustering results for departing relative motion trajectories near the example orbits at apolune and perilune are summarized in Table 6. The values are similar, but not exact, for both sets of relative trajectories at these locations as a result of the symmetry of the periodic orbits. For all non-circular orbits, more clusters and a higher percentage of noise are observed at apolune compared to perilune. This is consistent with the larger degree of geometric diversity seen at these locations. The relative motion clusters displayed in the following figures are all taken from a target state near apolune as a result.

Table 6. Summary of clustering results for departing relative motion trajectories at perilune (P) and apolune (A) for example periodic orbits.

Orbit	# of Clusters (P)	Noise (%) (P)	# of Clusters (A)	Noise (A)
L_2 Lyapunov Orbit	132	13.6	197	14.8
L_1 Halo Orbit	156	18.3	248	27.9
L_1 Vertical Orbit	179	22.6	262	19.3
L_2 Axial Orbit	178	24.3	272	19.3
L_2 Southern NRHO	200	12.5	317	51.7
Distant Prograde Orbit	229	26.9	235	27.3
Low Prograde Orbit	481	48.2	489	49.1
Distant Retrograde Orbit	362	30.5	365	30.7

Selected clusters of trajectories and their primitives for a target in an L_2 Lyapunov orbit near apolune are depicted in Figure 4. Many of these relative motion paths follow nearly straight lines with a low degree of curvature, as seen in the center column. This behavior is expected for a periodic orbit with highly unstable in-plane modes. Trajectories also remain mostly within the $x-y$ plane, with only moderate deviations observed in the clusters in the right column. This is consistent with the out-of-plane orbit stability characteristics. Relative motion paths exit or enter the target region from multiple directions in the $x-y$ plane, presenting a variety of options for trajectory design.

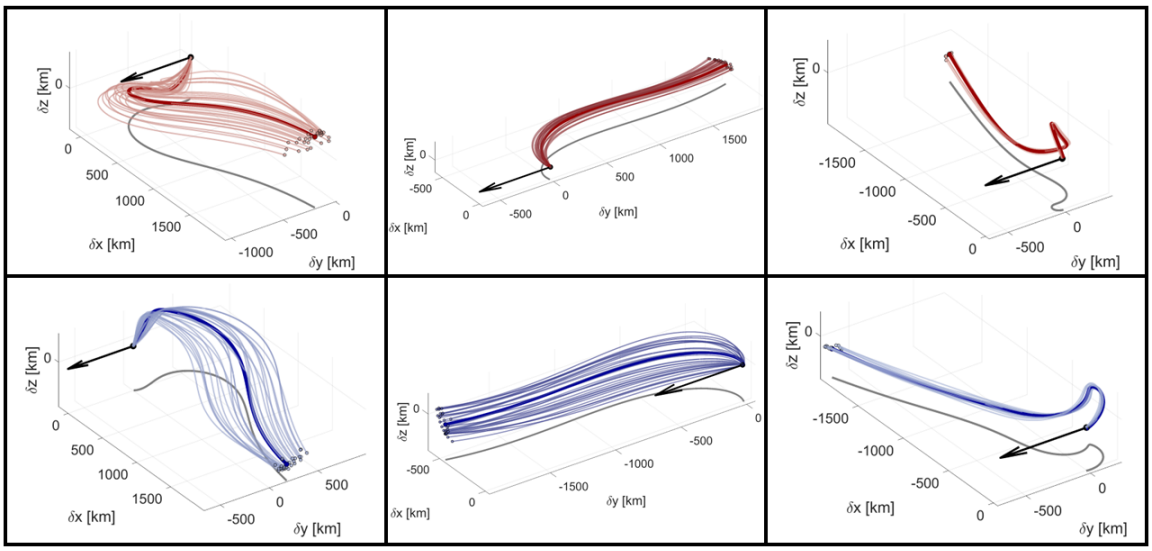

Figure 4. Clusters of departing (red) and approaching (blue) relative motion trajectories for a chaser spacecraft near a target spacecraft in an L_2 Lyapunov orbit at apolune.

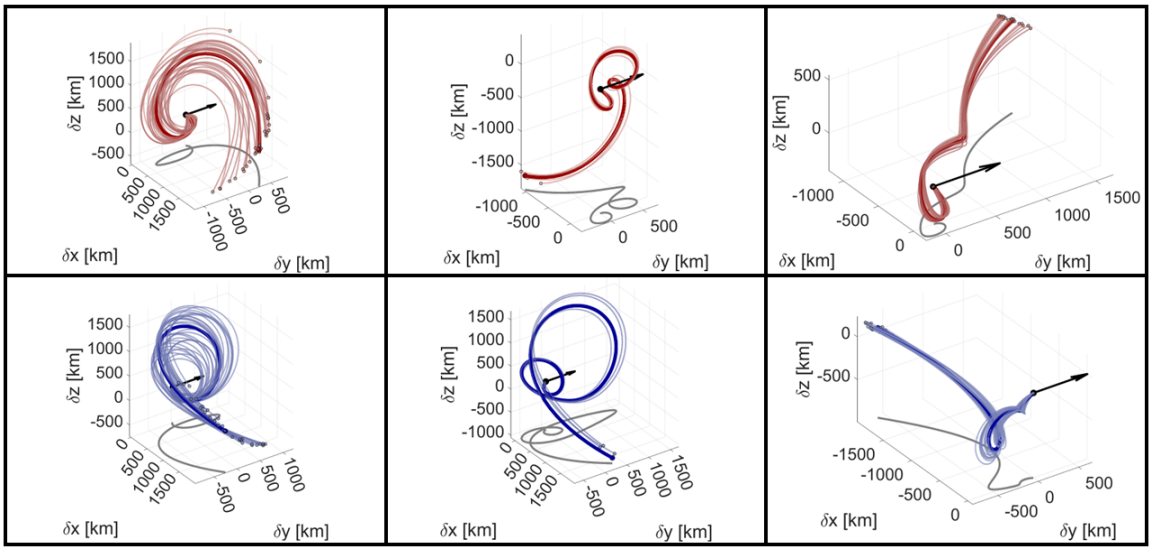

Figure 5. Clusters of departing (red) and approaching (blue) relative motion trajectories for a chaser spacecraft near a target spacecraft in an L_1 halo orbit at apolune.

Figure 5 depicts clusters of geometrically similar relative trajectories departing or arriving at an L_1 halo orbit for a target state at apolune. The leftmost clusters are the largest grouping of departure and approach clusters, with each one containing approximately 8% of all initial chaser conditions. Accordingly, the clustering approach can identify the common modes of behavior and summarize them with a motion primitive. Loops observed in the right two columns represent local minima and maxima of range with respect to the target identified by the curvature-based sampling approach.

Clusters of relative motion trajectories and their associated primitives for an L_1 vertical orbit and an L_2 axial orbit are displayed in Figure 6 and Figure 7 respectively. For the vertical orbit, faster

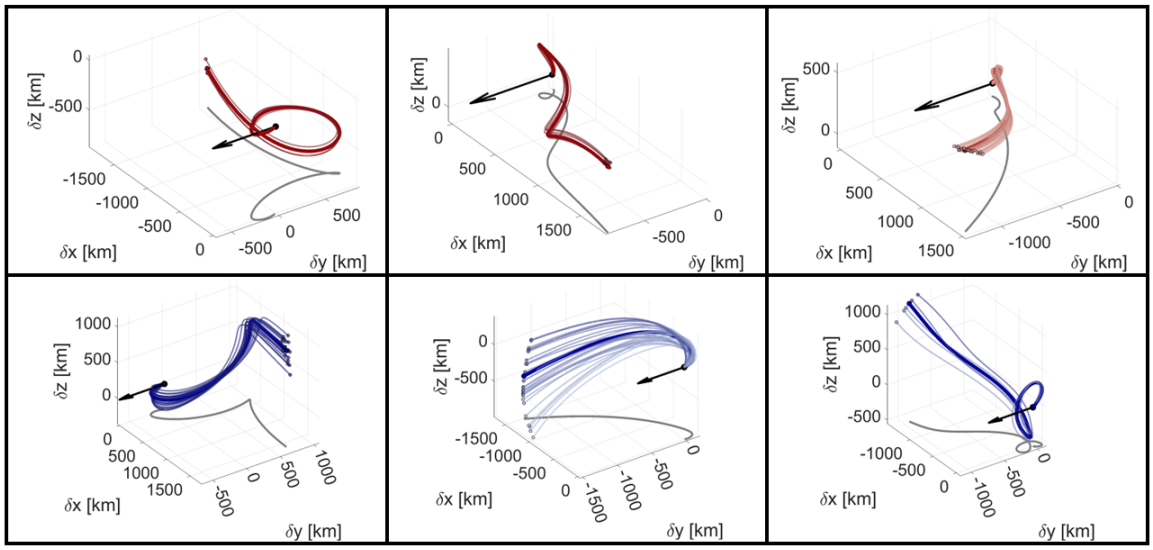

Figure 6. Clusters of departing (red) and approaching (blue) relative motion trajectories for a chaser spacecraft near a target spacecraft in an L_1 vertical orbit at apolune.

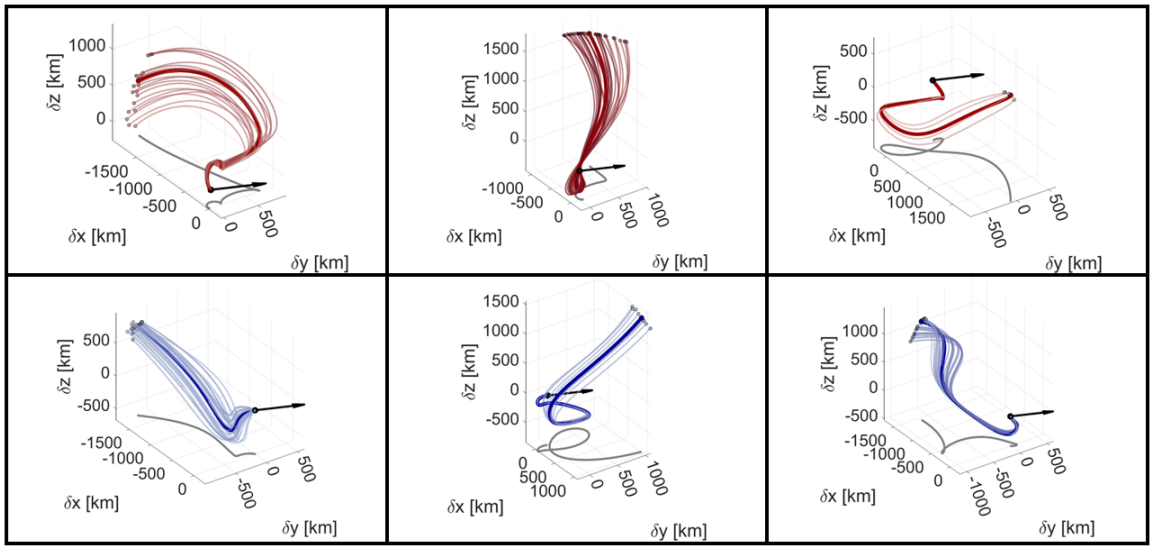

Figure 7. Clusters of departing (red) and approaching (blue) relative motion trajectories for a chaser spacecraft near a target spacecraft in an L_2 axial orbit at apolune.

approach trajectories are seen on the bottom left, with slower approaches in the center column as indicated by their respective shades. Although a more circuitous route might be associated with a slower velocity, the initial speeds associated with trajectories on the bottom right appear to be significantly faster. Departing trajectories for the axial orbit in Figure 7 demonstrate significantly different in-plane and out-of-plane behavior. While the top right cluster consists of relative motion mostly confined to the $x - y$ plane, the top middle trajectories travel along a nearly vertical path.

Trajectories are generated to approach or depart apolune on an L_2 southern near-rectilinear halo orbit (NRHO), similar to the baseline orbit for the Lunar Gateway.[1] Selected clusters of these relative trajectories are displayed in Figure 8. Due to the orientation of the NRHO, significantly less

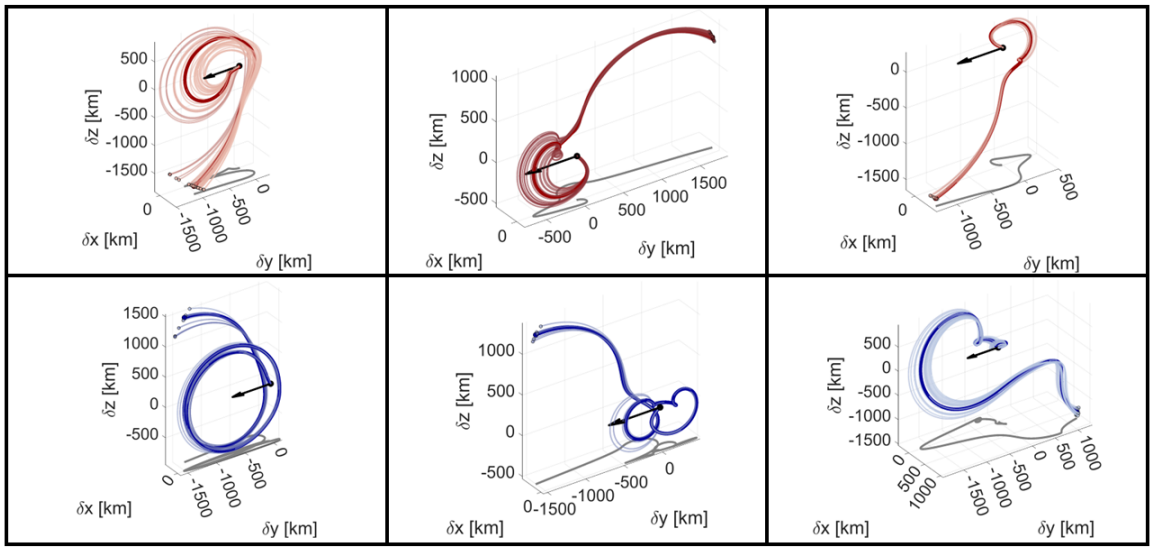

Figure 8. Clusters of departing (red) and approaching (blue) relative motion trajectories for a chaser spacecraft near a target spacecraft in an L_2 southern near-rectilinear halo (NRHO) orbit at apolune.

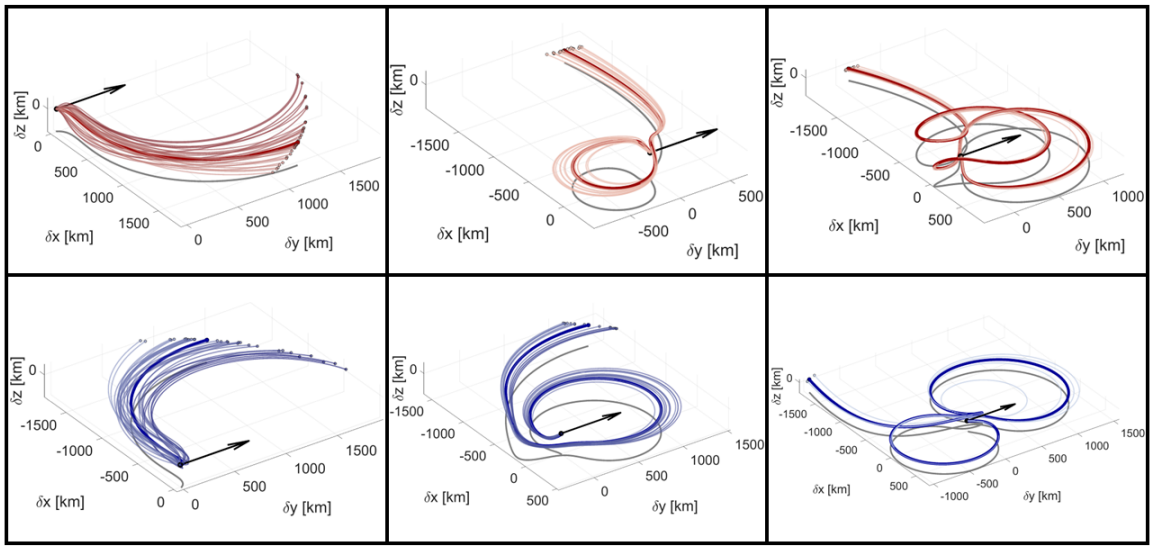

Figure 9. Clusters of departing (red) and approaching (blue) relative motion trajectories for a chaser spacecraft near a target spacecraft in a distant prograde orbit (DPO).

motion in the x direction is observed compared to the other orbits. These relative motions exhibit the widest variety of geometric diversity as a result of the nearly stable character of the NRHO. One of the significant risks for relative motion in this orbit is the risk of recontact with the target following departure.[25] Examples of this behavior appear in the two left departure trajectories, both of which feature close passes to the target. With the addition of uncertainty from ephemeris effects, these motion types may risk a potential collision. Trajectories like those observed on the top right could potentially reduce this risk. However, if trajectory design requirements made close passes on approach desirable, the bottom left two clusters may represent appropriate choices.

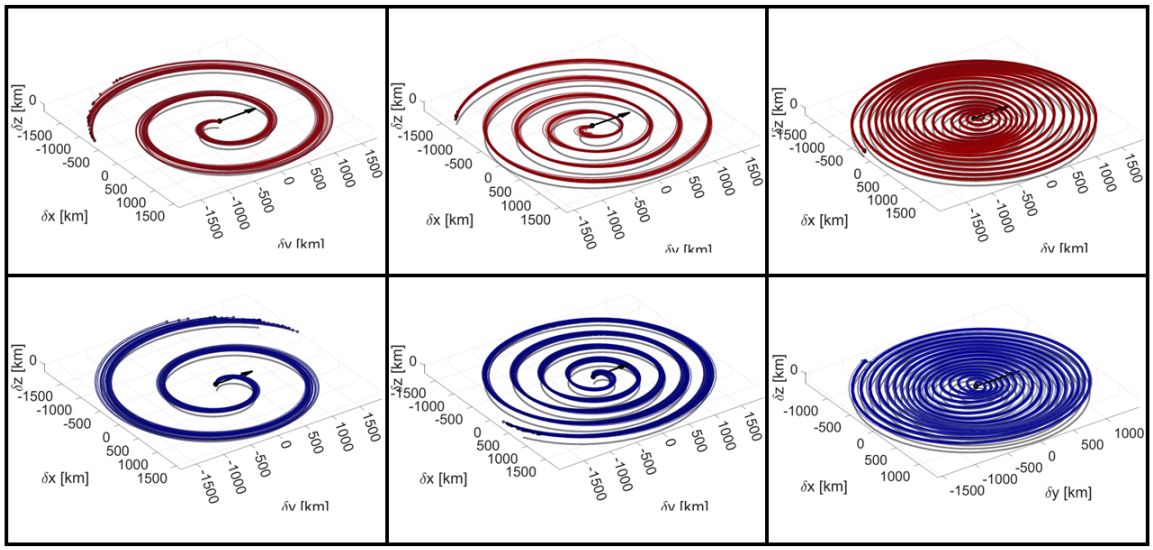

Figure 10. Clusters of departing (red) and approaching (blue) relative motion trajectories for a chaser spacecraft near a target spacecraft in a low prograde orbit (LoPO).

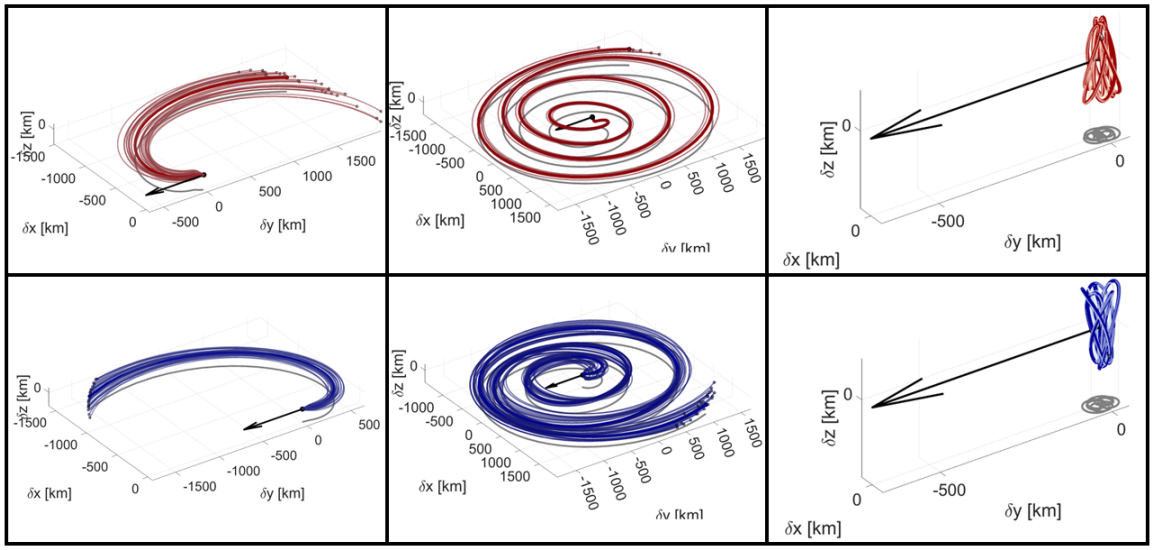

Figure 11. Clusters of departing (red) and approaching (blue) relative motion trajectories for a chaser spacecraft near a target spacecraft in distant retrograde orbit (DRO).

Relative motion trajectories near targets in planar periodic orbits centered about the Moon exhibit interesting behavior. Clusters for a distant prograde orbit (DPO) are shown in Figure 9. Many trajectories directly depart or approach the target region with a relatively high speed, as seen in the left column. Other classes of trajectories linger in the target region for significantly longer, with chaser spacecraft in the right column performing multiple loops with close passes by the target. Clusters of relative motion paths near a low prograde orbit (LoPO) are showcased in Figure 10. All of these trajectories resemble the spiral patterns observed with the DRO, with the number of rotations gradually increasing to exceedingly high values. The right column also features clusters

of trajectories with motion bounded near the target, which may also be associated with a quasi-periodic orbit (QPO). Finally, selected clusters near a distant retrograde orbit (DRO) are seen in Figure 11. As with the DPO, some trajectories rapidly depart or approach the target. The majority of the remaining trajectories gradually spiral out or in, with clusters representing various degrees of revolution and associated curvature events. However, some paths remain bounded near the target in trajectories that resemble a QPO, as seen in the right column.

Across each case, the relative motion primitives presented in this paper provide a summary of chaser spacecraft trajectories for a target spacecraft located along a periodic orbit. This behavior varies significantly depending on the type of periodic orbit, the target spacecraft's specific location along this periodic orbit, and the initial relative position and velocity of the chaser spacecraft. Although invariant manifolds can be used to predict behavior departing and approaching periodic orbits in the CR3BP, the diversity of geometry observed in these trajectories is more extensive. The application of relative motion primitives can be used to identify the most common modes of this behavior, select for desired initial or final conditions, or choose desired loitering characteristics near a target spacecraft. A more succinct summary of the complex relative paths in these environments could have multiple applications for rendezvous trajectory design, and is a focus of ongoing work.

CONCLUSION

This paper adapts motion primitives for astrodynamics applications to summarize relative trajectories near periodic orbits in cislunar space. These relative motion primitives capture geometrically distinct paths for a chaser spacecraft in the vicinity of a target spacecraft. First, target states are generated along periodic orbits in the vicinity of libration points L_1 and L_2 as well as the Moon. Chaser states are then generated to span the configuration space of relative positions and velocities around each target state. These conditions are then propagated forward and backward in time to produce departing and approaching sets of relative motion trajectories, taking samples at specified conditions using several criteria. The samples are arranged into feature vectors that are then used to cluster both sets of trajectories into geometrically similar groupings, and a representative motion primitive is extracted from each cluster. Through this approach, a library of chaser spacecraft trajectories is generated to summarize relative motion near selected target states along several periodic orbits. Future work includes aggregating relative motion clusters from multiple target states to identify regions of similar behavior along periodic orbits. A broader goal is to combine relative motion primitives with far-range motion primitives to design comprehensive rendezvous trajectories.

ACKNOWLEDGMENTS

This research was conducted at the University of Colorado Boulder under a NASA Space Technology Graduate Research Opportunity Fellowship from the National Aeronautics and Space Administration.

REFERENCES

[1] NASA, "NASA's Lunar Exploration Program Overview," *National Aeronautics and Space Administration*, 2020, pp. 1–75.

[2] W. H. Clohessy and R. S. Wiltshire, "Terminal guidance system for satellite rendezvous," *Journal of the Aerospace Sciences*, Vol. 27, No. 9, 1960, pp. 653–658.

[3] R. Luquette and R. Sanner, "Linear State-Space Representation of the Dynamics of Relative Motion, Based on Restricted Three Body Dynamics," *AIAA Guidance, Navigation, and Control Conference and Exhibit*, 2004, pp. 1–9.

[4] G. Franzini and M. Innocenti, "Relative Motion Dynamics in the Restricted Three-Body Problem," *Journal of Spacecraft and Rockets*, Vol. 56, No. 1, 2019, pp. 1–16.

[5] G. Franzini and M. Innocenti, "Relative motion equations in the local-vertical local-horizon frame for rendezvous in lunar orbits," *2017 AAS/AIAA Astrodynamics Specialist Conference*, 2017, pp. 1–15.

[6] K. Alfriend, S. R. Vadali, P. Gurfil, J. How, and L. Breger, *Spacecraft Formation Flying*. Elsevier, 1st ed., 2009.

[7] F. Hsiao and D. Scheeres, "The Dynamics of Formation Flight About a Stable Trajectory," *The Journal of the Astronautical Sciences*, Vol. 27, 2002, pp. 269–287.

[8] I. Elliott and N. Bosanac, "Describing relative motion near periodic orbits via local toroidal coordinates," *Celestial Mechanics and Dynamical Astronomy*, Vol. 134, No. 19, 2022, pp. 1–33.

[9] A. Wolek and C. A. Woolsey, *Model-Based Path Planning*. Springer International Publishing, 1st ed., 2017.

[10] E. Frazzoli, M. A. Dahleh, and E. Feron, "Real-Time Motion Planning for Agile Autonomous Vehicles," *Journal of Guidance, Control, and Dynamics*, Vol. 25, No. 1, 2004, pp. 1077–1091.

[11] T. Smith and N. Bosanac, "Constructing motion primitive sets to summarize periodic orbit families and hyperbolic invariant manifolds in a multi-body system," *Celestial Mechanics and Dynamical Astronomy*, Vol. 134, No. 7, 2022, pp. 1–33.

[12] T. Smith and N. Bosanac, "Motion Primitive Approach to Spacecraft Trajectory Design in a Multi-body System," *The Journal of the Astronautical Sciences*, Vol. 70, No. 34, 2023, pp. 1–47.

[13] C. Gillespie, G. Miceli, and N. Bosanac, "Summarizing Natural and Controlled Motion in Cislunar Space with Behavioral Motion Primitives," *AAS/AIAA Space Flight Mechanics Meeting*, 2025.

[14] G. E. Miceli and N. Bosanac, "Designing Neptunian System Tours via a Motion Primitive Approach," *AAS/AIAA Space Flight Mechanics Meeting*, 2025.

[15] V. Szebehely, *Theory of Orbits: The Restricted Problem of Three Bodies*. New York: Academic Press, Inc, 1967.

[16] K. Wardle, *Differential Geometry*. Mineola, NY: Dover Publications, Inc, 2008.

[17] N. Patrikalakis, T. Maekawa, and W. Cho, *Shape Interrogation for Computer Aided Design and Manufacturing*. Ebook, 2009.

[18] N. Bosanac, "Curvature Extrema Along Trajectories in the Circular Restricted Three-Body Problem," *2024 AAS/AIAA Astrodynamics Specialist Conference*, 2024.

[19] F. Klok, "Computer Aided Geometric Design," *Celestial Mechanics and Dynamical Astronomy*, Vol. 3, No. 3, 1986, pp. 217–229.

[20] J. Han, M. Kamber, and J. Pei, *Data Mining: Concepts and Techniques*. Waltham, MA: Morgan Kaufmann Publishers, 3rd ed., 2012.

[21] M. Ester, H.-P. Kriegel, J. Sander, and X. Xu, "A density-based algorithm for discovering clusters in large spatial databases with noise," *KDD'96: Proceedings of the Second International Conference on Knowledge Discovery and Data Mining*, 1996, pp. 226–231.

[22] R. J. Campello, D. Moulavi, and J. Sander, "Density-Based Clustering Based on Hierarchical Density Estimates," *Advances in Knowledge Discovery and Data Mining*, 2013, pp. 160–172.

[23] C. Malzer and M. Baum, "A Hybrid Approach To Hierarchical Density-based Cluster Selection," *2020 IEEE International Conference on Multisensor Fusion and Integration for Intelligent Systems,*, 2020, pp. 223–228.

[24] L. McInnes, J. Healy, and S. Astels, "hdbscan: Hierarchical density based clustering," *The Journal of Open Source Software*, Vol. 2, No. 11, 2017.

[25] D. Davis, E. Zimovan-Spreen, B. McCarthy, D. Henry, and K. Howell, "Cubesat Deployment from a Near Rectilinear Halo Orbit," *AIAA SCITECH 2022 Forum*, 2022.

[26] S. Scheuerle, D. Davis, E. Zimovan-Spreen, B. McCarthy, D. Henry, and K. Howell, "Jettison and Disposal from Near Rectilinear Halo Orbits, Part 1: Theory," *American Astronautical Society Astrodynamics Specialists Conference*, 2023.

[27] G. Bucchioni, M. D. Benedetti, F. D'Onofrio, and M. Innocenti, "Fully Safe Rendezvous Strategy in Cis-Lunar Space: Passive and Active Collision Avoidance," *The Journal of the Astronautical Sciences*, Vol. 69, 2022, pp. 1319–1346.

[28] P. Schulte, P. Spehar, and D. Woffinden, "GNC Sequencing for Orion Rendezvous, Proximity Operations, and Docking," *Annual AAS Guidance, Navigation and Control Conference*, 2020.

[29] N. Bosanac, "Data-Driven Summary of Motion in an Ephemeris Model of Cislunar Space," *AAS/AIAA Space Flight Mechanics Meeting*, 2025.

[30] Y. Zheng and X. Zhou, *Computing with Spatial Trajectories*. New York, NY: Springer, 2011.